



## Subtle microstructural changes of the cerebellum in a knock-in mouse model of DYT1 dystonia



Chang-Hyun Song<sup>a,1</sup>, Doug Bernhard<sup>a</sup>, Ellen J. Hess<sup>a,b</sup>, H.A. Jinnah<sup>a,c,d,\*</sup>

<sup>a</sup> Department of Neurology, Emory University, Atlanta 30322, GA, USA

<sup>b</sup> Department of Pharmacology, Emory University, Atlanta 30322, GA, USA

<sup>c</sup> Department of Human Genetics, Emory University, Atlanta 30322, GA, USA

<sup>d</sup> Department of Pediatrics, Emory University, Atlanta 30322, GA, USA

### ARTICLE INFO

#### Article history:

Received 9 September 2013

Accepted 2 October 2013

Available online 11 October 2013

#### Keywords:

Mouse mutant

Anatomy

Golgi histochemistry

Stereology

Cerebellum

Purkinje cells

Deep cerebellar neuron

Heterotopic cells

### ABSTRACT

The dystonias are a group of disorders characterized by involuntary twisting and repetitive movements. DYT1 dystonia is an inherited form of dystonia caused by a mutation in the *TOR1A* gene, which encodes torsinA. TorsinA is expressed in many regions of the nervous system, and the regions responsible for causing dystonic movements remain uncertain. Most prior studies have focused on the basal ganglia, although there is emerging evidence for abnormalities in the cerebellum too. In the current studies, we examined the cerebellum for structural abnormalities in a knock-in mouse model of DYT1 dystonia. The gross appearance of the cerebellum appeared normal in the mutant mice, but stereological measures revealed the cerebellum to be 5% larger in mutant compared to control mice. There were no changes in the numbers of Purkinje cells, granule cells, or neurons of the deep cerebellar nuclei. However, Golgi histochemical studies revealed Purkinje cells to have thinner dendrites, and fewer and less complex dendritic spines. There also was a higher frequency of heterotopic Purkinje cells displaced into the molecular layer. These results reveal subtle structural changes of the cerebellum that are similar to those reported for the basal ganglia in the DYT1 knock-in mouse model.

© 2013 Elsevier Inc. All rights reserved.

### Introduction

The dystonias comprise a group of disorders characterized by involuntary sustained or intermittent muscle contractions with abnormal postures or repetitive movements (Albanese et al., 2013). Dystonia may occur in isolation, or it may be combined with other neurological defects (Fung et al., 2013). One inherited cause for isolated dystonia involves deletion of a GAG codon in the *TOR1A* gene at the DYT1 locus, resulting in the loss of a single amino acid in torsinA (Ozelius et al., 1997). This protein is a member of the AAA+ family of ATPases, and it is thought to function as a molecular chaperone (Tanabe et al., 2009). However, the biochemical and cellular mechanisms by which the mutation leads to abnormal motor control in DYT1 dystonia remain unknown.

Delineating the regions of the nervous system that are most relevant for the expression of dystonia is important for guiding research regarding which neurons to target for more detailed investigation. Traditionally, dystonia has been linked with dysfunction of the basal ganglia (Hallett, 2006; Mink, 2006; Perlmuter and Mink, 2004; Peterson et al., 2010; Wichmann, 2008). However, recent studies have pointed to dysfunction of the cerebellum too (Avanzino and Abbruzzese, 2012; Filip et al., 2013; Neychev et al., 2011; Sadnicka et al., 2012; Zoons et al., 2011). TorsinA is expressed at high levels in most neurons of the cerebellum (Puglisi et al., 2013). Functional neuroimaging of human DYT1 dystonia has revealed abnormal metabolic activity of the cerebellum (Argyelan et al., 2009), and 2-deoxyglucose autoradiography has indicated abnormal cerebellar activity in a knock-in mouse model of DYT1 dystonia (Zhao et al., 2011). Although histological studies have revealed no gross structural abnormalities of the cerebellum in humans with DYT1 dystonia (Standaert, 2011) or its mouse models (Oleas et al., 2013), diffusion tensor tractography studies have implied subtle structural defects of cerebellar outflow pathways in both humans (Argyelan et al., 2009) and mice (Ulug et al., 2011).

In the current studies, subtle structural changes of the cerebellum were explored in a knock-in mouse model of DYT1 dystonia using a combination of quantitative stereological assessments of the volumes of its major compartments, stereological and morphometric assessments of the numbers and morphologies of Purkinje cells (PCs), granule

**Abbreviations:** ΔE, deletion of a single GAG codon in *TOR1A* gene; GC, granule cell; GCL, granule cell layer; MCL, molecular cell layer; WM, white matter; DCN, deep cerebellar nuclei; PC, Purkinje cell; AP, region from bregma in the anterior–posterior direction.

\* Corresponding author at: 6300 Woodruff Memorial Research Building, Department of Neurology, Emory University, Atlanta 30322, GA, USA.

E-mail address: [hjinnah@emory.edu](mailto:hjinnah@emory.edu) (H.A. Jinnah).

Available online on ScienceDirect ([www.sciencedirect.com](http://www.sciencedirect.com)).

<sup>1</sup> Present address: Department of Anatomy and Histology, College of Korean Medicine, Daegu Haany University, Gyeongsan, Republic of Korea, 712–715.

cells (GCs), and neurons of the deep cerebellar nuclei (DCN). The fine structure of PCs in Golgi stains was also examined by detailed morphometric evaluations. The results demonstrate multiple microstructural defects similar to those reported for neurons of the basal ganglia (Song et al., 2013). The results imply that mutations in *torsinA* have broad consequences for neuronal structure and function, and they raise questions regarding which of the consequences may be most relevant for the expression of abnormal movement in DYT1 dystonia.

## Materials & methods

### Animals

All experiments were carried out with approval of the Institutional Animal Care and Use Committee at Emory University. Heterozygous DYT1( $\Delta E$ ) mutant knock-in mice (Goodchild et al., 2005) were maintained congenically through crosses with the C57BL/6J strain (Jackson Laboratory, Bar Harbor, ME) and genotyped using a primer pair for the 34 base pair *loxP* site in the DYT1 mutant as described previously (Song et al., 2013). All mice were housed on a 12 h light/dark cycle with food and water ad libitum and used at 3 months of age.

### Stereological studies

Six DYT1 mutants (3 males and 3 females) and six controls (3 males and 3 females) were randomly selected from the breeding colony and used for quantitative stereological studies. After anesthetizing the mice with 2,2,2-tribromoethanol, they were perfused transcardially with a rinse solution consisting of 137 mM NaCl, 22.2 mM dextrose, 23.4 mM sucrose, 2 mM  $\text{CaCl}_2$  and 1.6 mM sodium cacodylate at pH 7.2. They then received 4% paraformaldehyde fix solution containing 117 mM sucrose and 67 mM sodium cacodylate at pH 7.2. The brain was removed from the skull and post-fixed with 4% paraformaldehyde for 16 h, and then stored in 67 mM sodium cacodylate. The brains were embedded within a gelatin matrix using the MultiBrain process (NeuroScience Associates, Knoxville TN), and serial coronal sections were cut at 40  $\mu\text{m}$  through the entire cerebellum. Every sixth section at 240  $\mu\text{m}$  intervals was thionin-stained for Nissl substance, yielding ~15 sections for each mouse.

All quantitative studies were conducted by a microscopist blinded to genotype. Sections were examined under an Olympus BX51 light microscope (Melville, NY) with a motorized stage (MAC5000, Ludl Electronic Products, Hawthorne, NY) controlled by a computer with Stereo Investigator software (MicroBrightField, Williston, VT). The size (volume) of the cerebellum was estimated using the Cavalieri method with a virtual grid spaced at 100  $\mu\text{m}$  across the regions of interest of each section with a 4 $\times$  objective. For this analysis separate measures were taken for the cerebellar granular cell layer (GCL), molecular cell layer (MCL) and cerebellar white matter (WM). The flocculus and paraflocculus were excluded because these regions often were stretched or torn during removal from the skull.

To count GCs, the entire GCL was outlined with a 10 $\times$  objective, and the cells were counted at 100 $\times$  using the optical fractionator method with a 12  $\mu\text{m}$  depth and 1  $\mu\text{m}$  top guard zone. The virtual frame size for GC counting was 8  $\times$  8  $\mu\text{m}$  in a grid size of 500  $\times$  1450  $\mu\text{m}$ . To count neurons in the DCN, the entire area was outlined with a 10 $\times$  objective, and the cells were counted at 60 $\times$  using the optical fractionator method with a 12  $\mu\text{m}$  depth and 1  $\mu\text{m}$  top guard zone. The virtual frame size was 80  $\times$  80  $\mu\text{m}$  in a grid size of 250  $\times$  250  $\mu\text{m}$ . All stereological measures yielded a Gundersen coefficient error of <0.1.

The total numbers of PCs also were estimated. Because of their laminar layout, systematic random sampling methods typical of stereological studies were not applied. Instead, all PCs were counted at two different levels at approximately  $-5.8$  mm and  $-6.8$  mm from the bregma in the anterior–posterior (AP) direction according to the mouse brain atlas (Paxinos and Franklin, 2001). For sections where the PC layer

appeared more than one cell thick because of a tangential plane of section, only PCs in direct contact with the MCL were counted. The length of the PC layer counted also was traced, and the numbers of PCs were divided by length to estimate PC density (PCs/mm). Heterotopic PCs, defined as large cells with staining characteristics of typical PCs but completely surrounded by molecular layer on all sides, were counted separately at 20 $\times$  through the entire cerebellum.

### Golgi histochemistry

Brains from 6 DYT1 mutants (3 males and 3 females) and 6 controls (3 males and 3 females) were randomly selected from the breeding colony and processed with the FD Rapid GolgiStain™ Kit (FD NeuroTechnologies, Baltimore, MD) as described previously (Song et al., 2013). Briefly, mice were decapitated, and the brain was removed rapidly. The unfixed brain was immersed in solution A containing potassium dichromate and mercuric chloride, and solution B containing potassium chromate for 2 weeks in the dark. The brains then were placed in sucrose for 48 h at 4 °C, and frozen-sectioned in the sagittal plane at 100  $\mu\text{m}$  using a Microm HM 440E sliding microtome (Microm, Walldorf, Germany). The sections were stained with a mixture consisting of solution D and E in distilled water for 15 min, and rinsed with distilled water 3 times. Sections were mounted on glass slides, dehydrated through graded alcohols, and cover-slipped with Permount.

Four PCs with complete staining of all dendrites near the mid-sagittal plane were chosen for each mouse (24 control neurons and 24 mutant neurons) for detailed analysis by a microscopist blinded to genotype. Each neuron was reconstructed by 3-dimensional digital tracing with NeuroLucida software (MicroBrightField, Williston, VT) and a Wacom Intuos 2 digitizing tablet connected with an Olympus BX51 microscope and a 60 $\times$  objective. Morphometric features of the cell soma and dendrites were determined by NeuroExplorer software version 10.21 as previously described (Mikolaenko et al., 2005; Song et al., 2013). Dendrite thicknesses, numbers and lengths were measured according to branch order. Branch order was defined as previously described (Mikolaenko et al., 2005; Song et al., 2013) with the first dendrites arising directly from the soma defined as the first branch order, and each branch point marking a successively higher order. For dendritic spines, twenty distal dendrites with length of >10  $\mu\text{m}$  were selected at random for each neuron, and dendritic spines were counted at 100 $\times$ . For counting, spines were defined as any discrete protrusion visibly connected to a dendrite (Mikolaenko et al., 2005; Song et al., 2013). The total spines were divided by the dendritic lengths and presented as a spine density (spines/ $\mu\text{m}$ ).

### Statistical analysis

All of the data are presented as mean  $\pm$  SEM. For stereological measurements and PC density, the data were examined by analysis of variance (ANOVA) with genotype and sex as potential explanatory variables. For morphometric data in Golgi histochemistry, 24 control and 24 mutant PCs were examined by ANOVA with genotype and sex as explanatory variables, and branch order was treated as a repeated measurement. The numbers of heterotopic PCs were examined by Kruskal–Wallis test for non-parametric data because of their small numbers. For all analyses, statistical significance was defined as  $p < 0.05$ .

## Results

### Gross cerebellar morphology

In keeping with prior studies of other DYT1 mouse models (Oleas et al., 2013), there were no obvious defects in the overall structure of the cerebellum, or the laminar arrangement of the GCL, MCL, or PC layer (Fig. 1). However, more precise evaluations of the different cerebellar compartments using stereological volumetric measures suggested

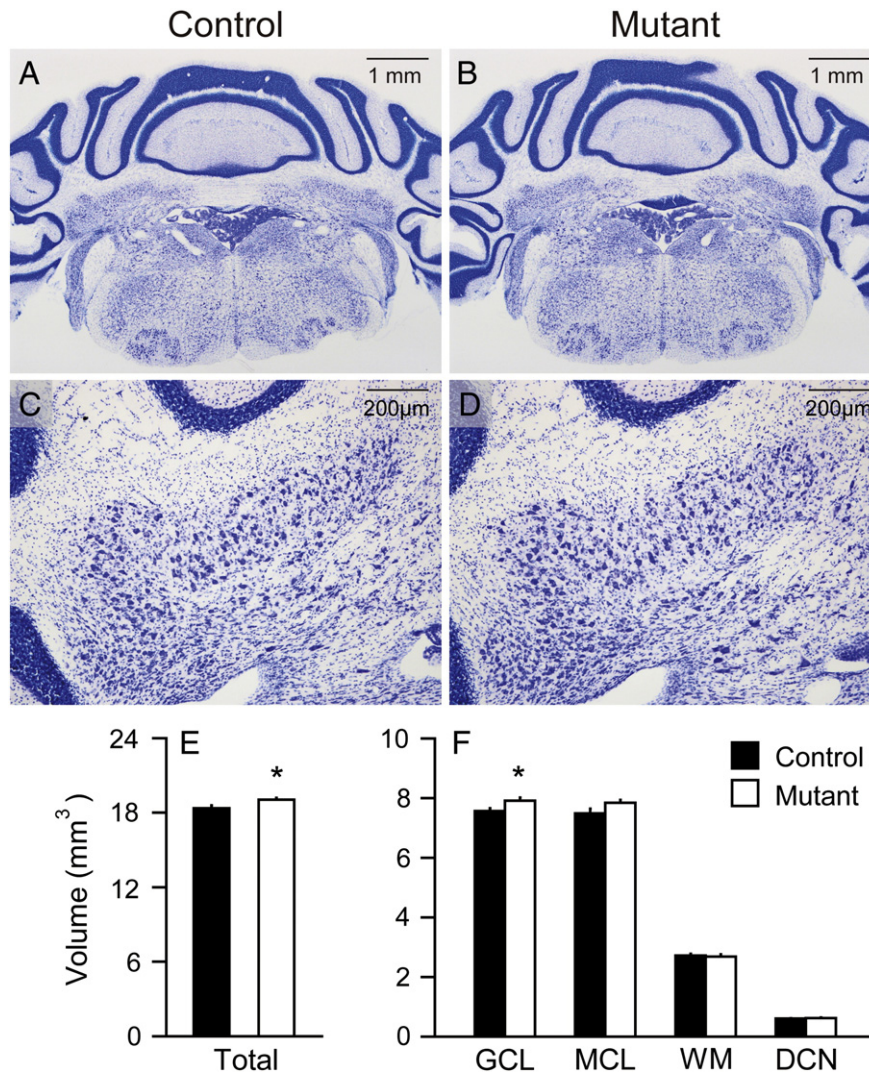


**Fig. 1.** Gross cerebellar structure. No obvious abnormalities were found in Nissl stains of the cerebellum between controls (A) and mutants (B). The distribution of deep cerebellar nucleus (DCN) neurons was not different between controls (C) and mutants (D). However, stereological measures of tissue volumes revealed mutants (white bars) to have 4% higher total cerebellar volumes and more specifically 5% higher granular cell layer compared to controls (black bars) (E–F). There were no significant increases in the volumes of the molecular cell layer (MCL), white matter (WM) or DCN. All data represent average values  $\pm$  SEM, and asterisks denote statistical significance at  $p < 0.05$ .

subtle enlargement of the cerebellum in the mutants. The data for regional volumes were examined by ANOVA with genotype, sex, and compartment (layer) as explanatory variables. There were significant main effects of genotype ( $F = 10.0$ ;  $p < 0.01$ ) and compartment ( $F = 4357.5$ ;  $p < 0.01$ ), but not for sex ( $F = 1.9$ ;  $p > 0.10$ ). There was a significant interaction between genotype and compartment ( $F = 3.3$ ;  $p < 0.05$ ), but no interaction between genotype and sex ( $F = 0.1$ ;  $p > 0.10$ ). The total volume of the cerebellum including GCL, MCL and DCN was slightly increased in the mutants, and post-hoc tests suggested a 5% increase specifically of the GCL volume ( $p < 0.05$ , Fig. 1F). Combining volumes across sex, total cerebellar volume was  $18.36 \pm 0.23 \text{ mm}^3$  in controls and  $19.05 \pm 0.13 \text{ mm}^3$  in mutants. For the individual compartments, the GCL volume was  $7.56 \pm 0.10 \text{ mm}^3$  in controls vs.  $7.91 \pm 0.10 \text{ mm}^3$  in mutants, the MCL was  $7.49 \pm 0.15 \text{ mm}^3$  in controls vs.  $7.84 \pm 0.10 \text{ mm}^3$  in mutants, the DCN was  $0.60 \pm 0.01 \text{ mm}^3$  in controls vs.  $0.62 \pm 0.02 \text{ mm}^3$  in mutants, and the WM was  $2.71 \pm 0.07 \text{ mm}^3$  in controls vs.  $2.68 \pm 0.07 \text{ mm}^3$  in mutants.

#### DCN neurons

DCN neurons receive inhibitory inputs from PCs and excitatory inputs from mossy fiber and climbing fibers, and are the major source of

output from the cerebellum. They were examined because of imaging studies suggesting abnormalities of cerebellar outflow pathways in human DYT1 dystonia and DYT1 knock-in mice (Argyelan et al., 2009; Ulug et al., 2011). No obvious abnormalities were found in the morphological features of mutant DCN neurons in Nissl stains (Figs. 2A–B). Stereological measures revealed similar numbers of total DCN neurons in mutants ( $15,779 \pm 700$  cells) compared with controls ( $16,923 \pm 601$  cells) (Fig. 2C). ANOVA showed no main effects of genotype ( $F = 1.63$ ;  $p > 0.10$ ) or sex ( $F = 0.29$ ;  $p > 0.10$ ) and no interaction between genotype and sex ( $F = 0.53$ ;  $p > 0.10$ ). The results suggest no apparent structural abnormality of the DCN in the DYT1 mutant mice.

#### GCs

GCs are the most numerous type of neuron in the entire brain. They were examined because of the stereological results above suggesting an increase in the volume of the GCL. There were no obvious morphological abnormalities of GCs in Nissl stains (Figs. 2D–E). Stereological counts of cells revealed a trend for increased GCs in mutants ( $23,837,563 \pm 1,772,047$ ) compared with controls ( $21,160,641 \pm 1,509,827$ ) but the difference was not statistically significant (Fig. 2F). ANOVA showed no



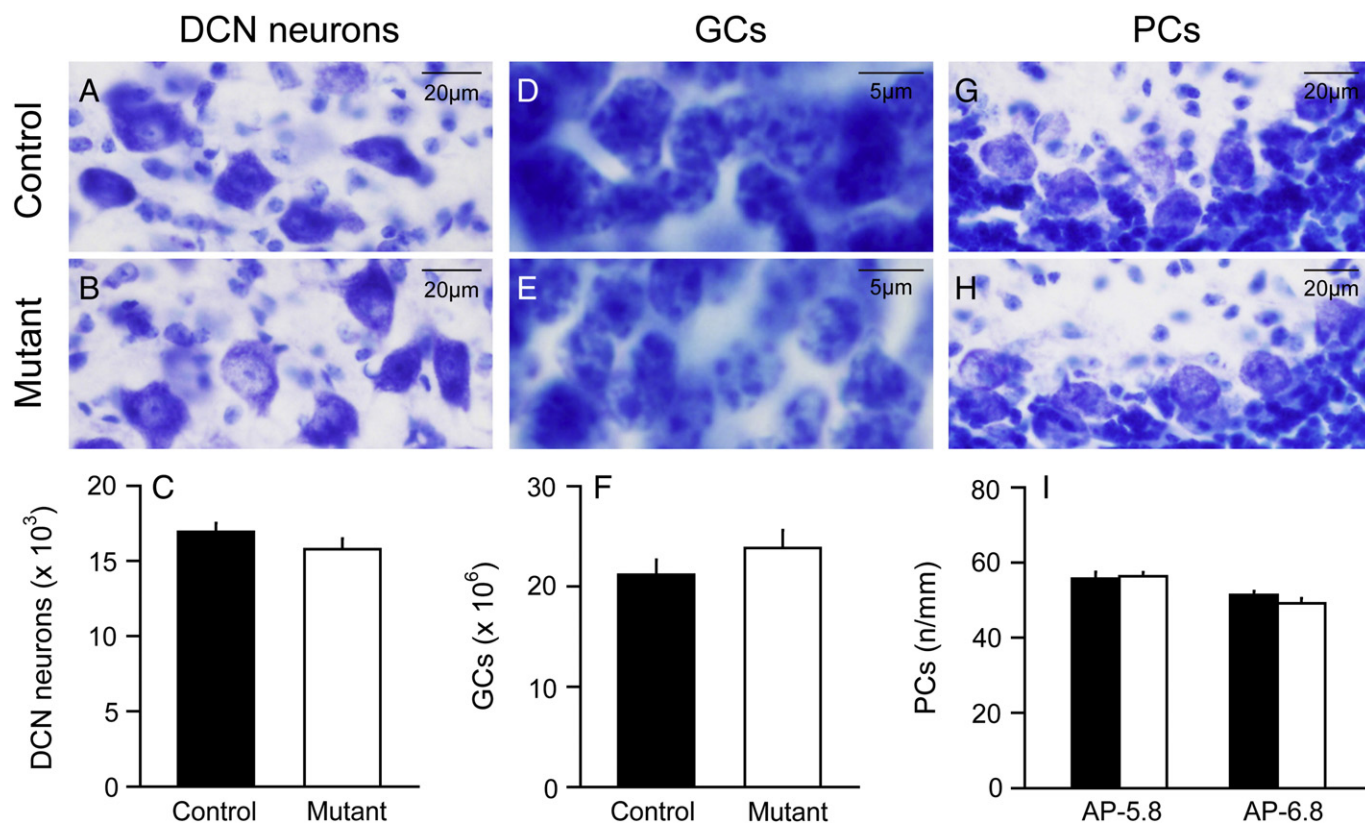


**Fig. 2.** Deep cerebellar nucleus neurons, granule cells and Purkinje cells. Deep cerebellar nucleus (DCN) neurons had similar morphologies in control (A) and mutant mice (B), and stereological counting revealed similar total numbers of DCN neurons in normal and mutant mice (C). Granule cells (GCs) also had similar morphologies in normal (D) and mutant (E) mice, and stereological studies revealed similar total numbers of GCs in normal and mutant mice (F). Purkinje cells (PCs) also had similar morphologies in normal (G) and mutant mice (H), and their linear density was similar in normal and mutant mice (I). In each graph, average results for control mice are shown with black bars and mutants with white bars. The error bars show standard error of the mean.

main effects of genotype ( $F = 2.0$ ;  $p > 0.10$ ) or sex ( $F = 4.9$ ;  $p > 0.10$ ) and no interaction between genotype and sex ( $F = 0.01$ ;  $p > 0.10$ ).

#### PCs

The PCs of the cerebellum play a major role in integrating inputs to the cerebellum and are the sole source of output from the cerebellar cortex. These neurons were explored in detail because of multiple studies suggesting an abnormal function or morphology of PCs in different types of dystonia (Neychev et al., 2008; Pizoli et al., 2002; Prudente et al., 2012; Raike et al., 2012). In keeping with prior studies, there were no obvious abnormalities in the layout or general appearance of these neurons in Nissl stains (Figs. 2G–H). PCs were counted at two levels (AP – 5.8 mm and AP – 6.8 mm), and the results were examined by ANOVA with genotype, sex and AP level as explanatory variables. For total counted PCs, there was a significant main effect of level ( $F = 6.4$ ;  $p < 0.05$ ) with 8% more cells at AP – 5.8 than AP – 6.8. However, there were no main effects of genotype ( $F = 0.2$ ;  $p > 0.10$ ) or sex ( $F = 2.4$ ;  $p > 0.10$ ). There were no interactions between genotype and sex ( $F = 0.01$ ;  $p > 0.10$ ) or genotype and level ( $F = 0.01$ ;  $p > 0.10$ ). Combining PCs across sex and section levels, there were  $1330 \pm 28$  PCs in controls and  $1349 \pm 36$  PCs in mutants. For total PC layer length measured, there were no main effects of genotype ( $F = 1.4$ ;  $p > 0.10$ ), sex ( $F = 0.07$ ;  $p > 0.10$ ), or level ( $F = 1.5$ ;  $p > 0.10$ ). There were no interactions between genotype and sex ( $F = 0.1$ ;  $p > 0.10$ ) or genotype and level ( $F = 1.2$ ;  $p > 0.10$ ). Combining cells across sex and section levels, the total PC layer length examined was  $24.9 \pm 0.4$  mm in controls and  $25.6 \pm 0.5$  mm in mutants.

When PC density was examined by dividing PC counts by total PC layer length, there were no main effects of genotype ( $F = 0.6$ ;  $p > 0.10$ ), sex ( $F = 2.3$ ;  $p > 0.10$ ), or level ( $F = 0.5$ ;  $p > 0.10$ ). There were no interactions between genotype and sex ( $F = 1.8$ ;  $p > 0.10$ ) or genotype and level ( $F = 0.6$ ;  $p > 0.10$ ). Combining PC density across sex and section levels, there were  $53.6 \pm 1.2$  cells/mm in controls vs.  $52.7 \pm 1.4$  cells/mm in mutants (Fig. 2I). These results suggest no obvious change in PC numbers or densities in the DYT1 mutants.

#### Heterotopic PCs

Heterotopic PCs are neurons that are abnormally displaced into the MCL from their normal location between the MCL and GCL (Fig. 3A). They were quantified because they are seen in a number of neurodevelopmental and neurodegenerative diseases (Gomez et al., 1997; Nakamura et al., 1999; Yamada et al., 2008). Since heterotopic PCs are sparse, they were counted in all sections from each cerebellum, with approximately 15 sections per mouse. There were 33% more heterotopic PCs in mutants ( $25.0 \pm 2.6$ ) compared to controls ( $18.8 \pm 2.0$ ), a difference that was statistically significant by the Kruskal–Wallis test for non-parametric measures (Fig. 3B;  $p < 0.05$ ). Heterotopic PCs in the mutants appeared to be more frequent in the caudal cerebellum compared to the anterior cerebellum (Figs. 3C–D), although they were too few for rigorous statistical comparisons.

#### Fine structure of PCs in Golgi histochemistry

In keeping with prior studies, PCs had large soma and extensive dendritic trees with considerable variation from cell to cell (Fig. 4). This

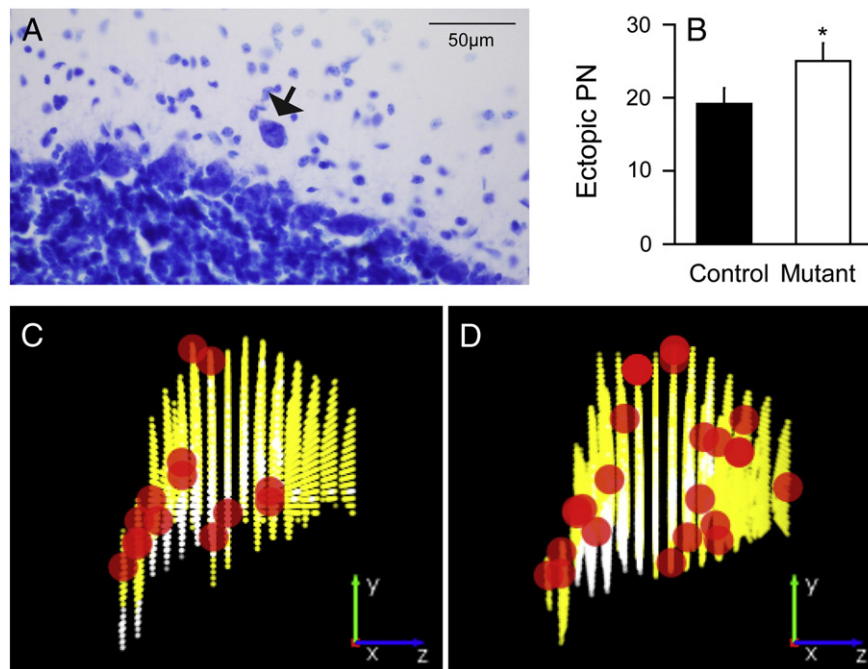


**Fig. 3.** Heterotopic Purkinje cells. Heterotopic Purkinje cells (PCs) were seen rarely in both normal and mutant mice (A, black arrow). The average number of heterotopic PCs ( $\pm$  SEM) was 33% higher in mutants (white bar) compared to controls (black bar) (B). Panels C and D show a 3-dimensional reconstruction of representative heterotopic PCs of controls and mutants, respectively, with X, Y and Z axes indicating medio-lateral, ventro-dorsal and antero-caudal directions, respectively, and the pictures are left-view of heterotopic cells (red) on 15 coronal sections marked for granular cell layer and molecular cell layer (yellow) and white matter (white). There was a trend that DYT1 mutants have the heterotopic cells distributed more in caudal cerebellum. Asterisk denotes statistical significance at  $p < 0.05$ .

variation made it difficult to identify any obvious differences between mutant and normal mice. To obtain more precise measures, 24 mutant and 24 normal PCs randomly selected in the midsagittal plane were digitally reconstructed by a microscopist blinded to genotype (Fig. 4). PC soma sizes were estimated by calculating total soma areas and perimeters from the digital traces. ANOVA with genotype and sex as potential explanatory variables revealed no significant main effect of genotype for area ( $F = 0.8$ ;  $p > 0.10$ ) or perimeter ( $F = 1.4$ ;  $p > 0.10$ ). There also were no significant effects for sex on area ( $F = 0.2$ ;  $p > 0.10$ ) or perimeter ( $F = 0.01$ ;  $p > 0.10$ ). There were no interactions between genotype and sex for area ( $F = 0.4$ ;  $p > 0.10$ ) or perimeter ( $F = 0.6$ ;  $p > 0.10$ ). Combining data across sex, soma area was  $446.4 \pm 20.0 \mu\text{m}^2$  in controls vs.  $421.8 \pm 20.1 \mu\text{m}^2$  in mutants. Soma perimeter was  $80.5 \pm 1.8 \mu\text{m}$  in controls vs.  $77.5 \pm 1.9 \mu\text{m}$  in mutants.

Although PCs had normal soma sizes and perimeters in the DYT1 mutants, digital reconstructions revealed subtle abnormalities among the dendritic trees (Fig. 5). Morphometric parameters (dendrite thickness, dendritic numbers and dendritic lengths) were examined by ANOVA with genotype and sex as explanatory variables, with branch order as a repeated measure. For dendrite thickness (Fig. 5A), ANOVA revealed main effects for genotype ( $F = 4.7$ ;  $p < 0.05$ ) and branch order ( $F = 221.2$ ;  $p < 0.01$ ), but not for sex ( $F = 1.2$ ;  $p > 0.10$ ). There were no interactions between genotype and branch order ( $F = 0.4$ ;  $p > 0.10$ ) or genotype and sex ( $F = 0.5$ ;  $p > 0.10$ ). For dendritic number (Fig. 5B), the effect for genotype showed a borderline trend for statistical significance ( $F = 2.9$ ;  $p = 0.09$ ). The effect of branch order was highly significant ( $F = 121.9$ ;  $p < 0.01$ ), but the effect of sex was not ( $F = 1.9$ ;  $p > 0.10$ ). There were significant interactions between genotype and branch order ( $F = 3.0$ ;  $p < 0.05$ ), but no interactions between genotype and sex ( $F = 0.3$ ;  $p > 0.10$ ). Post-hoc tests revealed fewer dendrites in the mutants compared to controls for branch orders 13–17 ( $p < 0.05$ ). For total dendritic lengths (Fig. 5C), ANOVA revealed significant main effects for branch order ( $F = 102.8$ ;  $p < 0.01$ ) and a trend of borderline significance for genotype ( $F = 3.4$ ;  $p = 0.07$ ) and sex ( $F = 3.9$ ;  $p = 0.05$ ). There were significant interactions between genotype and branch order ( $F = 3.0$ ;  $p < 0.05$ ), but no interactions between genotype and sex

( $F = 0.4$ ;  $p > 0.10$ ). Post-hoc tests revealed shorter total dendritic lengths for branch orders 13–17 ( $p < 0.05$ ), corresponding to the same levels where fewer dendrites were found. When dendritic lengths were normalized to dendritic numbers by calculating mean dendritic lengths for each branch order (Fig. 5D), ANOVA revealed significant main effects of branch order ( $F = 57.6$ ;  $p < 0.01$ ), but not for genotype ( $F = 0.07$ ;  $p > 0.10$ ) or sex ( $F = 0.3$ ;  $p > 0.10$ ). There were no interactions between genotype and branch order ( $F = 1.5$ ;  $p > 0.10$ ) or genotype and sex ( $F = 0.04$ ;  $p > 0.10$ ). These results imply that reduced dendritic lengths might be explained by the loss of dendritic numbers, rather than shorter dendrites at branch orders 13–17.

Dendritic spines are specialized protrusions from the surface of dendrites, and provide an important locus for synaptic inputs. They are dynamic structures that are modified through synaptic activity and various pathological states (Bonhoeffer and Yuste, 2002; Fiala et al., 2002), with morphology that varies from short stubby knobs to longer protrusions with mushroomed or bifurcated ends. The spines of PCs are sparse among primary and secondary dendrites, but dense in distal dendrites. Dendritic spines of PCs were morphologically variable in both control and mutant mice, but spines in mutant PC appeared thinner and less complex (Figs. 6A–D). Spines were counted for 20 distal dendrites randomly selected for each digitally reconstructed neuron, and normalized against total dendritic lengths to yield spine density in spines/ $\mu\text{m}$ . ANOVA revealed main effects of genotype ( $F = 37.8$ ;  $p < 0.01$ ) and sex, with 14% lower spine density in mutants compared to controls, and 5% lower spine density in females compared to males. However, there was no interaction between genotype and sex ( $F = 0.8$ ;  $p > 0.10$ ). Combining data across sex, spine density was  $2.00 \pm 0.03$  spines/ $\mu\text{m}$  in controls and  $1.76 \pm 0.02$  spines/ $\mu\text{m}$  in mutants. These morphometric studies suggest subtle alterations of PC dendrites and spines in the DYT1 mutant mice.

## Discussion

These analyses reveal subtle anatomical alterations in the cerebellum of a knock-in mouse model of DYT1 dystonia. The volume of cerebellum, especially the GCL, was increased in the mutant mice. There



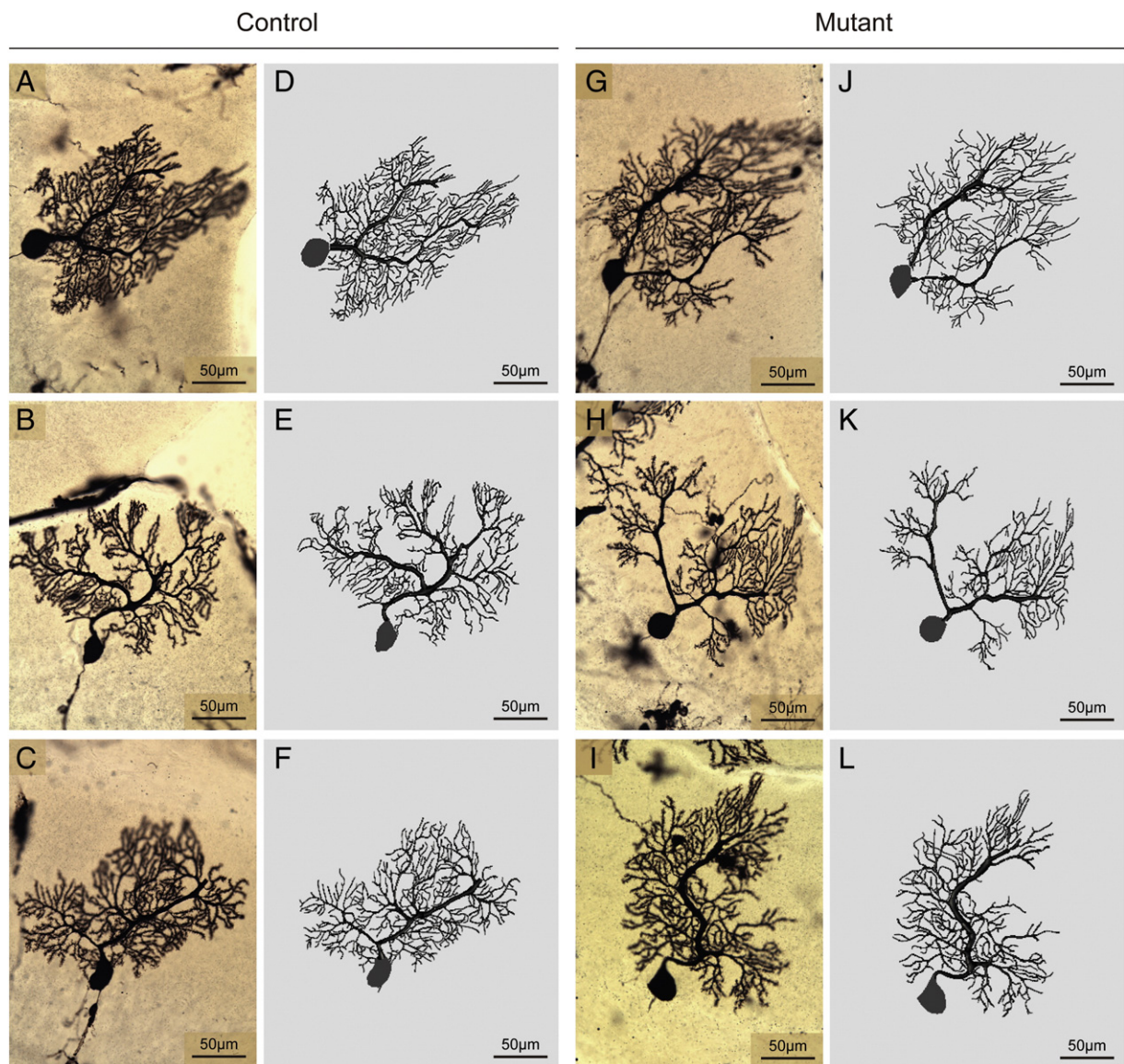


**Fig. 4.** Golgi histochemistry of Purkinje cells. The morphology of Purkinje cells (PCs) in Golgi stains was variable in both controls (A–C) and DYT1 mutants (G–I). The varied structures were more obvious in 3-dimensional digital tracings of controls (D–F) and mutants (J–L). In both groups of mice some PCs had a single major dendrite, while others had two or more. There were no overt structural differences between control and mutant mice.

were no differences in the numbers of DCN neurons, GCs or PCs between the controls and mutants, but mutants had more heterotopic PCs. In addition, mutant PCs had thinner and fewer dendrites with fewer and less complex spines. These findings are consistent with prior studies showing that torsinA is expressed at high levels in most cerebellar neurons (Puglisi et al., 2013), and other studies implying the metabolic and imaging abnormalities in this region in mouse models of DYT1 dystonia or affected humans. The results raise the possibility that anatomical abnormalities of the cerebellum may be related to the expression of dystonic movements.

#### *Subtle histological changes associated with DYT1 dystonia*

The current findings of subtle structural changes in the cerebellum in a DYT1 knock-in mouse model of dystonia are consistent with several other studies showing subtle structural changes in other regions of the DYT1 brain or its models. Although most histopathological studies of human DYT1 brains collected at autopsy show no obvious defects (Standaert, 2011), one study of 3 brains described ubiquitin-positive

inclusions in brainstem neurons (McNaught et al., 2004). Brainstem ubiquitin-positive inclusions also have been found in different rodent models of DYT1 dystonia (Dang et al., 2005; Grundmann et al., 2007; Shashidharan et al., 2005). At the ultrastructural level, several investigators have reported “blebs” of the nuclear envelope in several brain regions in mouse or rat models of DYT1 dystonia (Goodchild et al., 2005; Grundmann et al., 2007, 2012). These subtle structural abnormalities have led to the suggestion that defects of the nuclear envelope play a role in the expression of dystonia, and that DYT1 dystonia should be considered among disorders of the nuclear envelope, or the “nuclear envelopopathies”.

Another subtle anatomical finding has been a slight enlargement of dopaminergic neurons of the substantia nigra for both humans with DYT1 dystonia (Rostasy et al., 2003) and a knock-in mouse model (Song et al., 2012). A recent study described multiple subtle structural abnormalities in the striatum of a DYT1 knock-in mouse model including enlarged cholinergic and parvalbumin-positive interneurons, and a reduction in dendritic complexity and spines among GABAergic medium spiny projection neurons (Song et al., 2013). Additionally, a diffusion

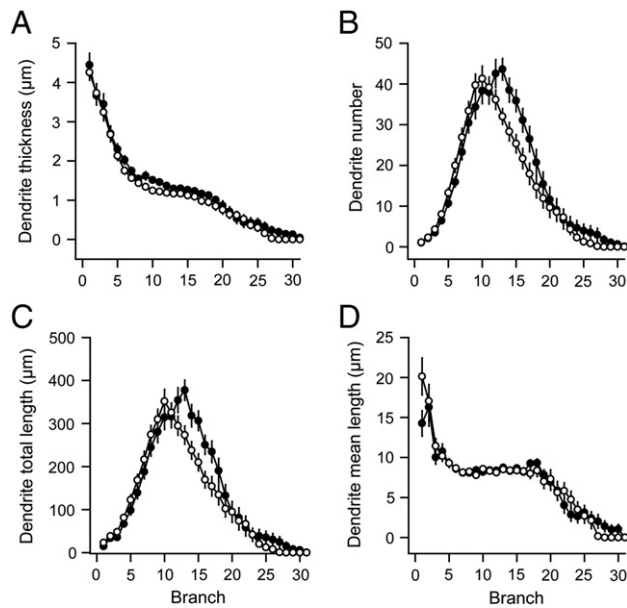


**Fig. 5.** Dendritic structure of Purkinje cells. Dendritic structure was evaluated according to branch order for both normal (closed circles) and DYT1 mutant mice (open circles). Data represent average values  $\pm$  SEM for 24 PCs from controls and 24 PCs from mutants. Mutant PC dendrites were generally thinner regardless of branch order (A). There were fewer dendrites at branch orders 13–17 in mutant PCs compared to controls (B). Total dendritic lengths also were shorter at branch orders 13–17 in mutant PCs compared to controls (C), but the mean lengths of dendrites were not different between controls and mutants (D).

tension imaging study implied abnormal connections between the cerebellum and thalamus (Ulug et al., 2011). Some of the subtle structural features examined in the current studies were also examined in a prior study of another DYT1 mouse model (Zhang et al., 2011). However, the anatomical assessments in this prior study were limited to measurements of the proximal dendrite of Purkinje cells and dendritic spines at the fourth branch order of these neurons in Golgi-stained material. While the more detailed results of the current study cannot be directly compared to this study because of multiple methodological differences, it is interesting to note that shorter proximal dendrites and fewer spines were found in both studies. Other studies have shown abnormal neurite outgrowth in culture models of DYT1 dystonia (Hewett et al., 2006). Taken together, all of these anatomical findings support suggestions that the expression of motor dysfunction in DYT1 dystonia is related to abnormal neuronal signaling, and that it may be considered a “synaptopathy” rather than a “nuclear envelopathy” (Granata et al., 2009; Warner et al., 2010).

In addition to subtle defects in the nuclear envelope, neuronal soma, dendrites and spines, the increase in heterotopic PCs suggests that abnormal locations of neurons may also occur. Heterotopic PCs are not specific to DYT1 dystonia, since they have been observed in other neurodevelopmental and degenerative disorders (Gomez et al., 1997; Kuo et al., 2011; Nakamura et al., 1999; Yamada et al., 2008). A subtle redistribution of subpopulations of striatal neurons also was observed in a prior study of the DYT1 mouse model studied here (Song et al., 2013), and defects in neuronal migration have been described for a DYT1 knockout model (McCarthy et al., 2012). How these many subtle anatomical abnormalities in different cellular compartments and brain regions may be related to each other remains to be established. However, the finding of structural abnormalities, even subtle ones, helps to provide clues to the cellular and regional defects responsible for DYT1 dystonia. Subtle structural anomalies appear to exist in different cellular compartments for human DYT1 dystonia or its animal models in the brainstem, midbrain, striatum, and cerebellum. The current findings

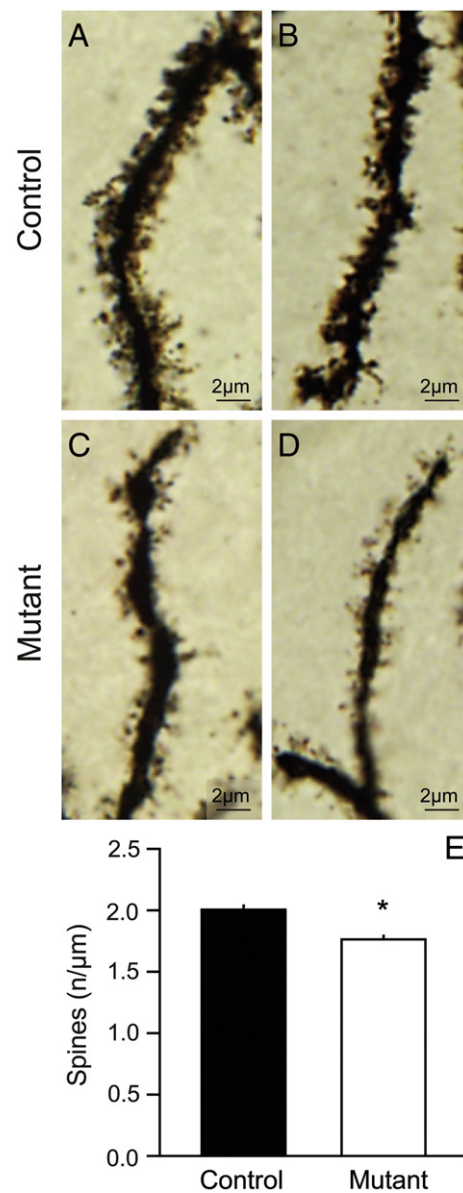


**Fig. 6.** Dendritic spines of Purkinje cells. In Golgi stains, dendritic spines appeared denser and more complicated in control (A–B) compared to DYT1 mutant mice (C–D). The data in panel E show average spine densities  $\pm$  SEM for 20 randomly selected distal dendrites from each of 24 control PCs ( $n = 480$  dendrites, black bar) and the same number of mutant PCs ( $n = 480$  dendrites, white bar). The density of dendritic spines was 12% reduced in DYT1 mutants. Asterisk denotes statistical significance at  $p < 0.05$ .

add to the list of subtle structural alterations that may be caused by abnormal torsinA.

The numerous subtle structural abnormalities are not surprising, given the apparent role of torsinA in numerous different cellular processes and widespread expression in the brain (Augood et al., 1999; Konakova and Pulst, 2001; Konakova et al., 2001; Shashidharan et al., 2000; Xiao et al., 2004). As summarized in several recent reviews (Granata et al., 2009; Tanabe et al., 2009), torsinA is thought to function as a molecular chaperone, participating in the folding and translocation of various proteins in different cellular compartments. It interacts with numerous proteins, with consequences in the nuclear envelope, endoplasmic reticulum, neurites, and synapse. These functions may translate into subtle structural abnormalities such as abnormal cell sizes or changes in neurites or their spinous processes. Further work is needed to decipher which cellular compartment and brain regions are most relevant for causing dystonia.



### Relevance to imaging studies of DYT1 dystonia

The histological studies also are relevant to understand the results of prior imaging studies of human DYT1 dystonia. Although there are no overt structural defects in routine clinical imaging studies, one voxel-based morphometric study of DYT1 dystonia suggested reduced volumes of the striatum (Draganski et al., 2009). Additionally, numerous functional imaging studies have revealed abnormalities in several brain regions. Studies of regional blood flow or regional metabolic activity via positron-emission tomography have revealed abnormalities in several cortical areas, striatum, and cerebellum (Carbon et al., 2004, 2008, 2010; Detante et al., 2004; Eidelberg et al., 1998). Finally, a diffusion tensor imaging study suggested an abnormal connectivity in pathways connecting cerebellum, thalamus and cortex (Argyelan et al., 2009).

While these human imaging studies imply that some subtle structural defects may occur in the human DYT1 brain, obtaining histological evidence defining the exact defects in the human brain has been elusive. Human autopsy specimens are difficult to obtain, because the disorder is very rare. Additionally, the types of abnormalities so far uncovered in animal models require methods that are not usually applied to human brains. For example, subtle changes in neuronal sizes will require quantitative comparisons of DYT1 brains with appropriately matched controls using rigorous stereological or morphometric measurements. Subtle changes in dendrites or spines require special histological methods, such as Golgi histochemistry, which are rarely applied to human specimens. Nevertheless, the results from animals point to the types of abnormalities that may have to be examined to obtain a more complete understanding of the histological basis for the imaging abnormalities reported.

### Structure and function in DYT1 dystonia

Although multiple subtle structural abnormalities have been described for DYT1 dystonia, their functional consequences remain unclear. Some of these changes may reflect pathological consequences of mutant torsinA, some may reflect compensatory adaptive changes, and others may be inconsequential. Considering that PC dendrites and spines are a critical locus for integrating inputs into the cerebellar cortex and determining PC output, it seems likely that a loss of dendrites and spines would be associated with altered cerebellar signaling. Thus structural defects among PC dendrites and spines could cause abnormal cerebellar signaling and abnormalities in motor control. On the other hand, dendrites and spines are highly plastic even in the normal brain, with dramatic adaptive changes in response to many normal physiological inputs. Thus structural abnormalities among PC dendrites may also be an adaptive change that reflects a pathological process in some distant brain region.

For DYT1 dystonia, there are numerous physiological studies demonstrating abnormal cortico-striatal signaling (Calabresi et al., 1997; Centonze et al., 2003; Martella et al., 2009; Pisani et al., 2006; Sciamanna et al., 2012a, 2012b), but there are no similar studies addressing cerebellar signaling. However, several studies of other animal models of dystonia have demonstrated an important causal role for abnormal cerebellar signaling. Dystonic movements in the *Dt* mutant rat are associated with abnormal cerebellar signaling, and surgical removal of the cerebellum or selective destruction of the DCN eliminates their dystonic movements (LeDoux et al., 1993, 1995, 1998). Dystonic movements in the tottering mouse model of paroxysmal dystonia also are associated with abnormal cerebellar signaling (Chen et al., 2009), and surgical removal of the cerebellum or selective elimination of PCs also eliminates their dystonic movements (Campbell et al., 1999; Neychev et al., 2008; Raïke et al., 2012; Shirley et al., 2008). Dystonic movements can even be elicited in normal rodents by local disruption of cerebellar signaling (Alvarez-Fischer et al., 2012; Pizoli et al., 2002; Raïke et al., 2012), an effect that seems to be mediated by glutamate receptors

(Fan et al., 2012). Electrophysiological studies of the cerebellum are clearly needed in DYT1 models to determine if the histological abnormalities are associated with aberrant cerebellar signaling, and delineating which of the many structural and functional alterations is most relevant for causing abnormal movements is an important challenge for future research.

### Acknowledgments

We thank Dr. William Dauer for making the DYT1 knock-in mice available for these studies. This work was supported in part by the Dystonia Medical Research Foundation, NIH grants NS040470 and NS033592.

### References

- Albanese, A., et al., 2013. Phenomenology and classification of dystonia: a consensus update. *Mov. Disord.* 28, 863–873.
- Alvarez-Fischer, D., et al., 2012. Prolonged generalized dystonia after chronic cerebellar application of kainic acid. *Brain Res.* 1464, 82–88.
- Argyelan, M., et al., 2009. Cerebellothalamocortical connectivity regulates penetrance in dystonia. *J. Neurosci.* 29, 9740–9747.
- Augood, S.J., et al., 1999. Distribution of the mRNAs encoding torsinA and torsinB in the normal adult human brain. *Ann. Neurol.* 46, 761–769.
- Avanzino, L., Abbruzzese, G., 2012. How does the cerebellum contribute to the pathophysiology of dystonia. *Basal Ganglia* 2, 231–235.
- Bonhoeffer, T., Yuste, R., 2002. Spine motility: phenomenology, mechanisms, and function. *Neuron* 35, 1019–1027.
- Calabresi, P., et al., 1997. Endogenous adenosine mediates the presynaptic inhibition induced by aglycemia at corticostriatal synapses. *J. Neurosci.* 17, 4509–4516.
- Campbell, D.B., et al., 1999. Tittering mouse motor dysfunction is abolished on the Purkinje cell degeneration (*pcd*) mutant background. *Exp. Neurol.* 160, 268–278.
- Carbon, M., et al., 2004. Regional metabolism in primary torsion dystonia: effects of penetrance and genotype. *Neurology* 62, 1384–1390.
- Carbon, M., et al., 2008. Increased cerebellar activation during sequence learning in DYT1 carriers: an equiperformance study. *Brain* 131, 146–154.
- Carbon, M., et al., 2010. Increased sensorimotor network activity in DYT1 dystonia: a functional imaging study. *Brain* 133, 690–700.
- Centonze, D., et al., 2003. Distinct roles of D1 and D5 dopamine receptors in motor activity and striatal synaptic plasticity. *J. Neurosci.* 23, 8506–8512.
- Chen, G., et al., 2009. Low-frequency oscillations in the cerebellar cortex of the tottering mouse. *J. Neurophysiol.* 101, 234–245.
- Dang, M.T., et al., 2005. Generation and characterization of Dyt1 deltaGAG knock-in mouse as a model for early-onset dystonia. *Exp. Neurol.* 196, 452–463.
- Detante, O., et al., 2004. Globus pallidus internus stimulation in primary generalized dystonia: a H<sub>2</sub>O PET study. *Brain* 127, 1899–1908.
- Draganski, B., et al., 2009. Genotype–phenotype interactions in primary dystonias revealed by differential changes in brain structure. *Neuroimage* 47, 1141–1147.
- Eidelberg, D., et al., 1998. Functional brain networks in DYT1 dystonia. *Ann. Neurol.* 44, 303–312.
- Fan, X., et al., 2012. Selective and sustained alpha-amino-3-hydroxy-5-methyl-4-isoxazolepropionic acid receptor activation in cerebellum induces dystonia in mice. *J. Pharmacol. Exp. Ther.* 340, 733–741.
- Fiala, J.C., et al., 2002. Dendritic spine pathology: cause or consequence of neurological disorders. *Brain Res. Rev.* 39, 29–54.
- Filip, P., et al., 2013. Dystonia and the cerebellum: a new field of interest in movement disorders? *Clin. Neurophysiol.* 124, 1269–1274.
- Fung, V.S., et al., 2013. Assessment of the patient with dystonia: an update on dystonia syndromes. *Mov. Disord.* 28, 889–898.
- Gomez, C.M., et al., 1997. Spinocerebellar ataxia type 6: gaze-evoked and vertical nystagmus, Purkinje cell degeneration, and variable age of onset. *Ann. Neurol.* 42, 933–950.
- Goodchild, R.E., et al., 2005. Loss of the dystonia-associated protein torsinA selectively disrupts the neuronal nuclear envelope. *Neuron* 48, 923–932.
- Granata, A., et al., 2009. TorsinA and dystonia: from nuclear envelope to synapse. *J. Neurochem.* 109, 1596–1609.
- Grundmann, M., et al., 2007. Overexpression of human wildtype torsinA and human deltaGAG torsinA in a transgenic mouse model causes phenotypic abnormalities. *Neurobiol. Dis.* 27, 190–206.
- Grundmann, K., et al., 2012. Generation of a novel rodent model for DYT1 dystonia. *Neurobiol. Dis.* 47, 61–74.
- Hallett, M., 2006. Pathophysiology of dystonia. *J. Neural Transm. Suppl.* 70, 485–488.
- Hewett, J.W., et al., 2006. Dystonia-causing mutant torsinA inhibits cell adhesion and neurite extension through interference with cytoskeletal dynamics. *Neurobiol. Dis.* 22, 98–111.
- Konakova, M., Pulst, S.M., 2001. Immunocytochemical characterization of torsin proteins in mouse brain. *Brain Res.* 922, 1–8.
- Konakova, M., et al., 2001. Cellular distribution of torsin A and torsin B in normal human brain. *Arch. Neurol.* 58, 921–927.
- Kuo, S.H., et al., 2011. Increased number of heterotopic Purkinje cells in essential tremor. *J. Neurol. Neurosurg. Psychiatry* 82, 1038–1040.



- LeDoux, M.S., et al., 1993. Cerebellectomy eliminates the motor syndrome of the genetically dystonic rat. *Exp. Neurol.* 120, 302–310.
- LeDoux, M.S., et al., 1995. Selective elimination of cerebellar output in the genetically dystonic rat. *Brain Res.* 697, 91–103.
- LeDoux, M.S., et al., 1998. Single-unit activity of cerebellar nuclear cells in the awake genetically dystonic rat. *Neuroscience* 86, 533–545.
- Martella, G., et al., 2009. Impairment of bidirectional synaptic plasticity in the striatum of a mouse model of DYT1 dystonia: role of endogenous acetylcholine. *Brain* 132, 2336–2349.
- McCarthy, D.M., et al., 2012. Neurogenesis and neuronal migration in the forebrain of the TorsinA knockout mouse embryo. *Dev. Neurosci.* 34, 366–378.
- McNaught, K.S., et al., 2004. Brainstem pathology in DYT1 primary torsion dystonia. *Ann. Neurol.* 56, 541–547.
- Mikolaenko, I., et al., 2005. A Golgi study of neuronal architecture in a genetic mouse model for Lesch–Nyhan disease. *Neurobiol. Dis.* 20, 479–490.
- Mink, J.W., 2006. Abnormal circuit function in dystonia. *Neurology* 66, 959.
- Nakamura, R., et al., 1999. An immunohistochemical study of Purkinje cells in a case of hereditary cerebellar cortical atrophy. *Acta Neuropathol.* 97, 196–200.
- Neychev, V., et al., 2008. The basal ganglia and cerebellum interact in the expression of dystonic movement. *Brain* 131, 2499–2509.
- Neychev, V.K., et al., 2011. The functional neuroanatomy of dystonia. *Neurobiol. Dis.* 42, 185–201.
- Oleas, J., et al., 2013. Engineering animal models for dystonia: what have we learned? *Mov. Disord.* 28, 990–1000.
- Ozelius, L.J., et al., 1997. The early-onset torsion dystonia gene (DYT1) encodes an ATP-binding protein. *Nat. Genet.* 17, 408.
- Paxinos, G., Franklin, K.B.J., 2001. *The Mouse Brain in Stereotaxic Coordinates*. Academic Press, San Diego.
- Perlmuter, J.S., Mink, J.W., 2004. Dysfunction of dopaminergic pathways in dystonia. *Adv. Neurol.* 94, 163–170.
- Peterson, D.A., et al., 2010. Convergent evidence for abnormal striatal synaptic plasticity in dystonia. *Neurobiol. Dis.* 37, 558–573.
- Pisani, A., et al., 2006. Altered responses to dopaminergic D2 receptor activation and N-type calcium currents in striatal cholinergic interneurons in a mouse model of DYT1 dystonia. *Neurobiol. Dis.* 24, 318–325.
- Pizoli, C.E., et al., 2002. Abnormal cerebellar signaling induces dystonia in mice. *J. Neurosci.* 22, 7825–7833.
- Prudente, C.N., et al., 2012. Neuropathology of cervical dystonia. *Exp. Neurol.* 241, 95–104.
- Puglisi, F., et al., 2013. Torsin A localization in the mouse cerebellar synaptic circuitry. *PLoS One* 8, e6803.
- Raibe, R.S., et al., 2012. Limited regional cerebellar dysfunction induces focal dystonia in mice. *Neurobiol. Dis.* 49, 200–210.
- Rostasy, K., et al., 2003. TorsinA protein and neuropathology in early onset generalized dystonia with GAG deletion. *Neurobiol. Dis.* 12, 11–24.
- Sadnicka, A., et al., 2012. The cerebellum in dystonia—help or hindrance? *Clin. Neurophysiol.* 123, 65–70.
- Sciamanna, G., et al., 2012a. Cholinergic dysregulation produced by selective inactivation of the dystonia-associated protein torsinA. *Neurobiol. Dis.* 47, 416–427.
- Sciamanna, G., et al., 2012b. Cholinergic dysfunction alters synaptic integration between thalamostriatal and corticostriatal inputs in DYT1 dystonia. *J. Neurosci.* 32, 11991–12004.
- Shashidharan, P., et al., 2000. Immunohistochemical localization and distribution of torsinA in normal human and rat brain. *Brain Res.* 853, 197–206.
- Shashidharan, P., et al., 2005. Transgenic mouse model of early-onset dyt1 dystonia. *Hum. Mol. Genet.* 14, 125–133.
- Shirley, T.L., et al., 2008. Paroxysmal dyskinesias in mice. *Mov. Disord.* 23, 259–264.
- Song, C.H., et al., 2012. Functional analysis of dopaminergic systems in a DYT1 knock-in mouse model of dystonia. *Neurobiol. Dis.* 48, 66–78.
- Song, C.H., et al., 2013. Subtle microstructural changes of the striatum in a DYT1 knock-in mouse model of dystonia. *Neurobiol. Dis.* 54, 362–371.
- Standaert, D.G., 2011. Update on the pathology of dystonia. *Neurobiol. Dis.* 42, 148–151.
- Tanabe, L.M., et al., 2009. Primary dystonia: molecules and mechanisms. *Nat. Rev. Neurol.* 5, 598–609.
- Ulug, A.M., et al., 2011. Cerebellothalamocortical pathway abnormalities in torsinA DYT1 knock-in mice. *Proc. Natl. Acad. Sci. U. S. A.* 108, 6638–6643.
- Warner, T.T., et al., 2010. TorsinA and DYT1 dystonia: a synaptopathy? *Biochem. Soc. Trans.* 38, 452–456.
- Wichmann, T., 2008. Commentary: dopaminergic dysfunction in DYT1 dystonia. *Exp. Neurol.* 212, 242–246.
- Xiao, J., et al., 2004. Developmental expression of rat torsinA transcript and protein. *Brain Res. Dev. Brain Res.* 152, 47–60.
- Yamada, M., et al., 2008. CAG repeat disorder models and human neuropathology: similarities and differences. *Acta Neuropathol.* 115, 71–86.
- Zhang, L., et al., 2011. Altered dendritic morphology of Purkinje cells in Dyt1 DeltaGAG knock-in and purkinje cell-specific Dyt1 conditional knockout mice. *PLoS One* 6, e18357.
- Zhao, Y., et al., 2011. The DYT1 carrier state increases energy demand in the olivocerebellar network. *Neuroscience* 177, 183–194.
- Zoons, E., et al., 2011. Structural, functional and molecular imaging of the brain in primary focal dystonia—a review. *Neuroimage* 56, 1011–1020.